Phys 777
Plasma Physcis and Magnetohydrodynamics
2004 Fall
Instructor: Dr. Haimin Wang

Lecture 8

Solar Flares

Solar Flares

- Flares are most violent form energy release. They always occur at magnetic neutral lines. They are observed in Hα, microwares, EUV, X-ray and Hard X-ray.
- X-ray classification: A,B,C, M,X (A,B: subflare)

Morphology:

- Single loop --- compact, short lived
- Two Ribbon --- long duration events, usually big

Basic Theory: Magnetic Reconnection

- Current sheets may be found in neutral lines and reconnect due to:

  (1) resistive instability, such as tearing mode

  (2) neutral line collapses due to separate flux systems are pushed together

  (3) sudden enhancement of resistivity

- Steady reconnection process is governed by:

  Ohm's law: $E + \vec{v} \times \vec{B} = \eta \nabla \times \vec{B}$

  Equation of motion: $\rho(\vec{v} \cdot \nabla)\vec{v} = -\nabla p + \nabla \times B \times \frac{B}{\mu}, \qquad \nabla \cdot B = 0$

  Continuity Equation: $\nabla \cdot (\rho \vec{v}) = 0$

1.4.4A. Basic Description

The optical flare is most often observed in Hα, formed in the low chromosphere. It has two basic stages. During the *flash phase*, which lasts typically 5 min (but sometimes an hour), the intensity and area of the emission rapidly increase in value. Then, in the *main phase*, the intensity slowly declines over about an hour (though sometimes as much as a day).

However, the flare is probably initiated and the energy released in a high-temperature region above the cool Hα flare. This overlying region of coronal loops may be heated to tens of millions of degrees; it exhibits variations co-incident with the flash and main phases, but also shows two more distinct phases. As seen in Figure 1.36, the soft X-ray emission (< 10 keV) possesses a *preflare phase* for minutes (or possibly longer) before flare onset, because of an enhanced thermal emission from the coronal plasma. Also, for 100 to 1000 s at the start of the flare, an *impulsive phase* is sometimes present, as indicated by the appearance of a microwave burst and a hard X-ray burst (> 30 keV) caused by highly accelerated electrons. After the impulsive phase, some

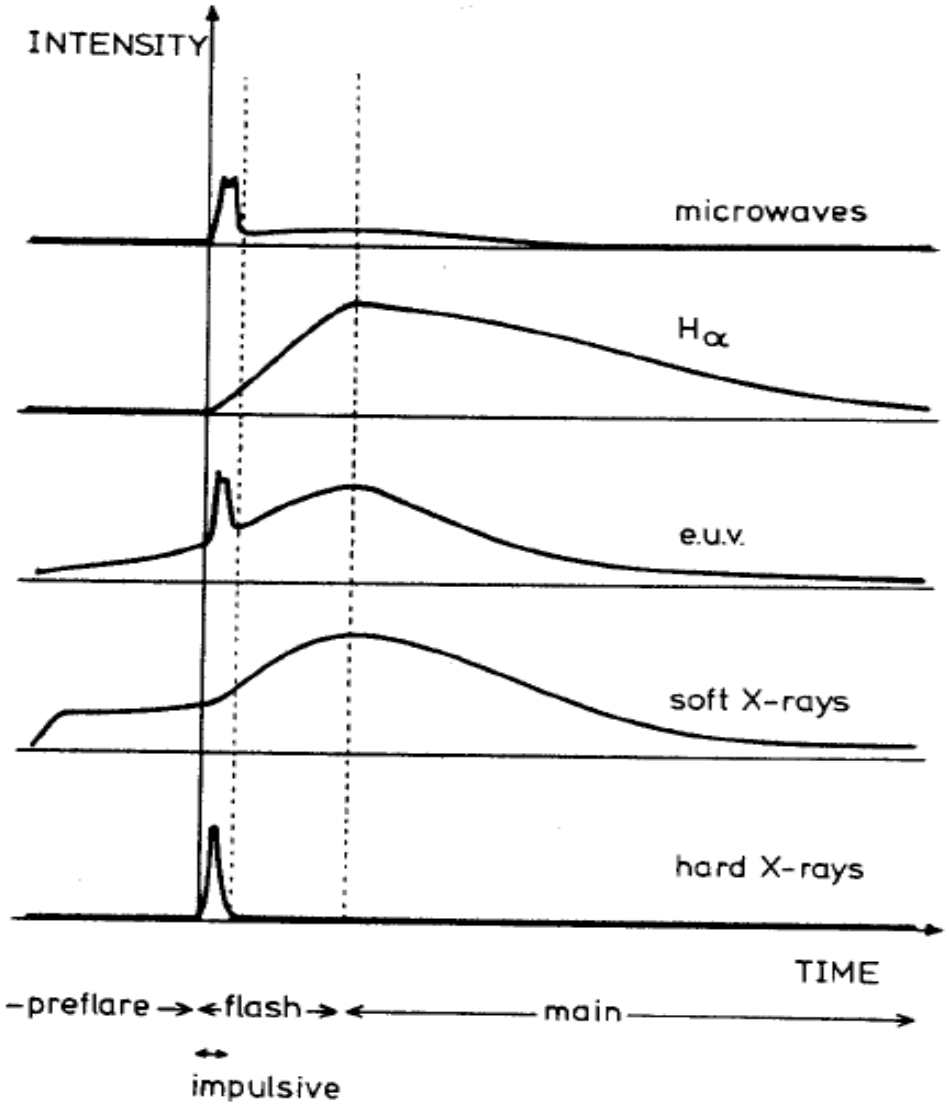

Fig. 1.36. A schematic profile of the flare intensity in several wavelengths (see, e.g., Kane, 1974; Lin, 1974). There is a great variation in the duration and complexity of the various phases. In a large event the pre-flare phase lasts typically 10 min, the impulsive phase a minute, the flash phase 5 min, and the main phase an hour.

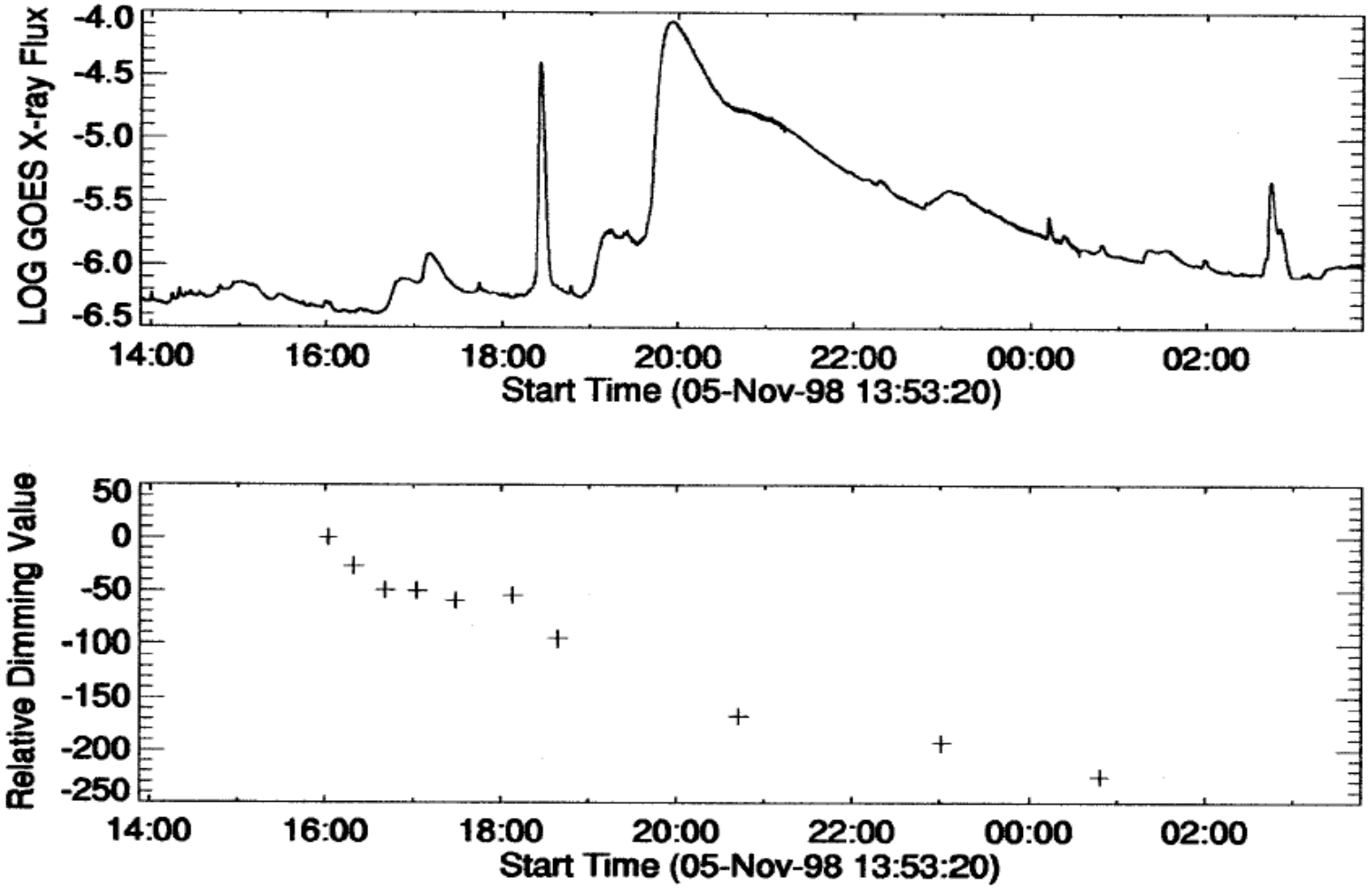

Fig. 2.— Top panel: GOES X-ray time profile of November 5, 1998 flare. Bottom panel: EUV dimming of the flare. The value is the contrast integrated over the entire dimming areas, in the unit of $10^{17}cm^2$.

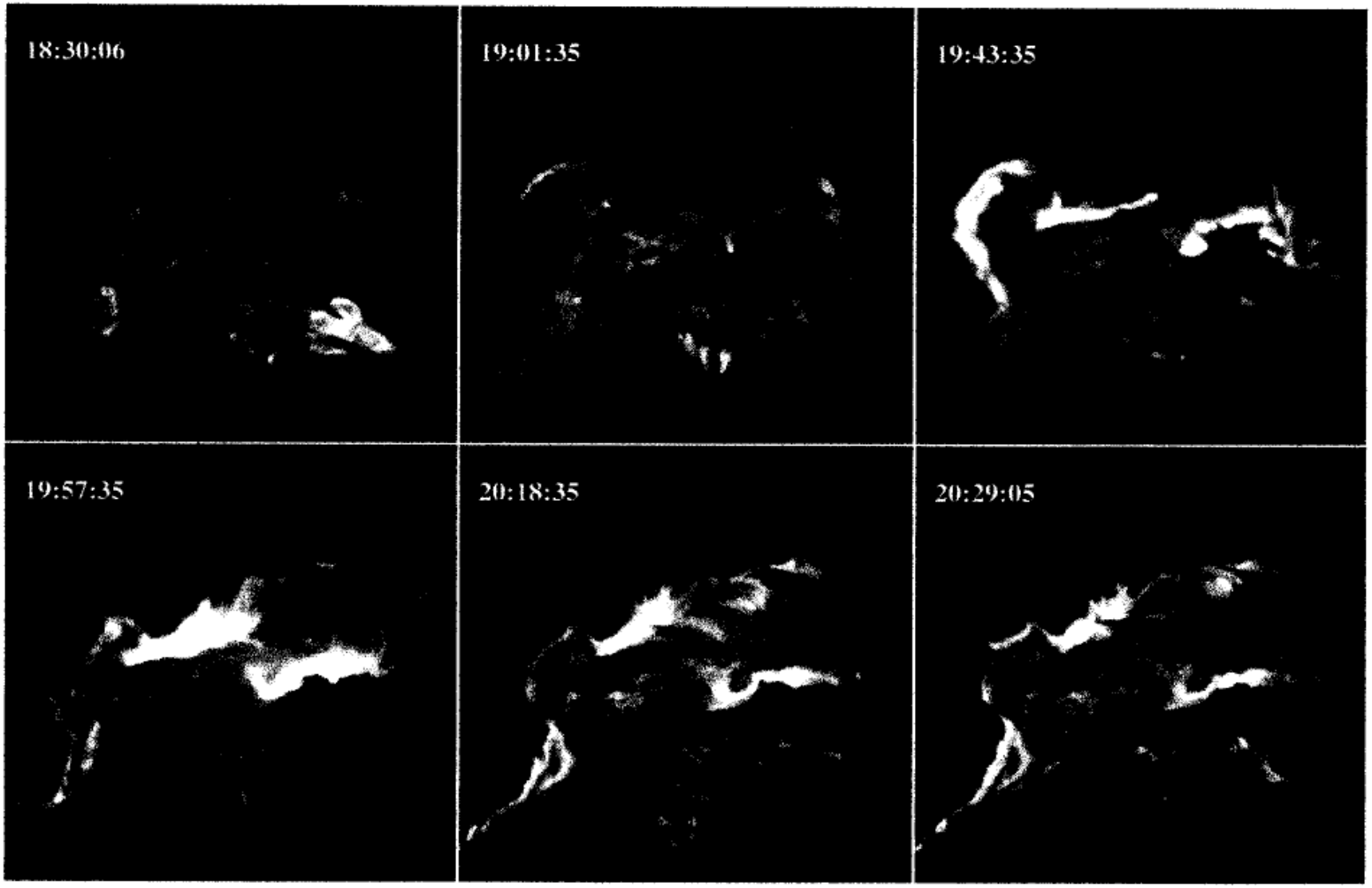

Fig. 4.— Time sequence of Hα observations of November 5, 1998. The images are from 65-cm telescope, the field of view is 200 by 200 arcsec.

Unidirectional Fields

$$v_x = -v_0 \frac{x}{a}, \qquad v_y = -v_0 \frac{y}{a}, \qquad B = B(x)\hat{y}$$

$$p = const - \frac{1}{2}\rho v^2 - \frac{B^2}{2\mu}$$

$$E - \frac{v_0 x}{a} B = \eta \frac{dB}{dx}$$

- If diffusion is absent, $\eta=0$ $B= Ea/v_0 x$
- If diffusion is present, then inside diffusion region field can slip through the plasma
- The width of the diffusion region is derived by

$$\frac{v_0 x}{a} B = \eta \frac{dB}{dx}, \qquad l = (\frac{\eta}{a v_0})^{1/2} a = \frac{L}{R_m^{1/2}}$$

In Fig 10.3, B_i are carried in, B_0 are carried out $\longrightarrow$ reconnection.

$B_0 < B_i$ Some energy is lost by heating and kinetic energy.

- Parker derived $v_0 = v_A^* = \dfrac{B_i}{(\mu\rho_c)^{1/2}}, \qquad v_i = \dfrac{\eta}{l}$

$$\rho_i v_i L = \rho_c v_0 l \qquad l << L \quad if \quad v_i << v_A^*(\rho_c / \rho_i)$$

- Pressure balance:

$$\rho_c = \rho_i + B_i^2 / 2\mu$$

$$\frac{\rho_c}{\rho_i} = \frac{T_i}{T_c}(1 + \beta_i)$$

In reality. We have to consider the ratio between radiation and convection

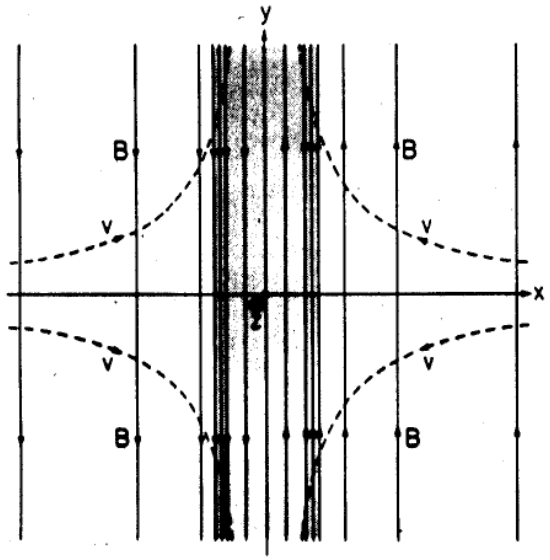

(a)

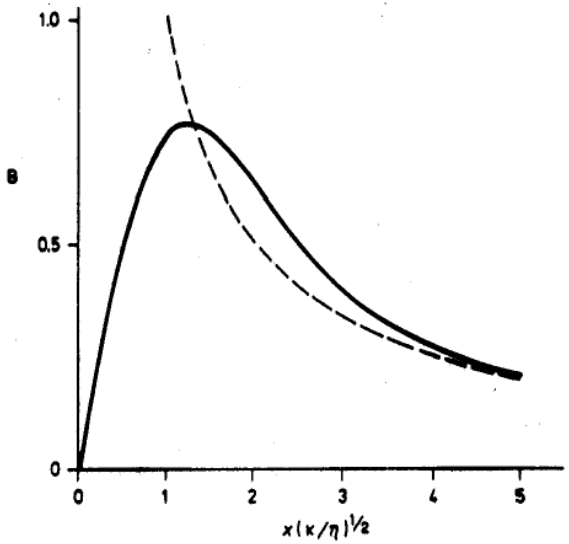

(b)

Fig. 10.2. Magnetic annihilation in a current sheet. (a) Oppositely directed magnetic field lines (——) are carried in from two sides by a stagnation point flow with streamlines (- - - - -). In the diffusion region (shaded) the field is no longer frozen to the plasma and magnetic energy is converted into heat by ohmic dissipation. (b) The field strength (B) as a function of x with $k = V_0/a$, expressed in units such that dB/dx is unity at $x = 0$ (from Priest and Sonnerup, 1975).

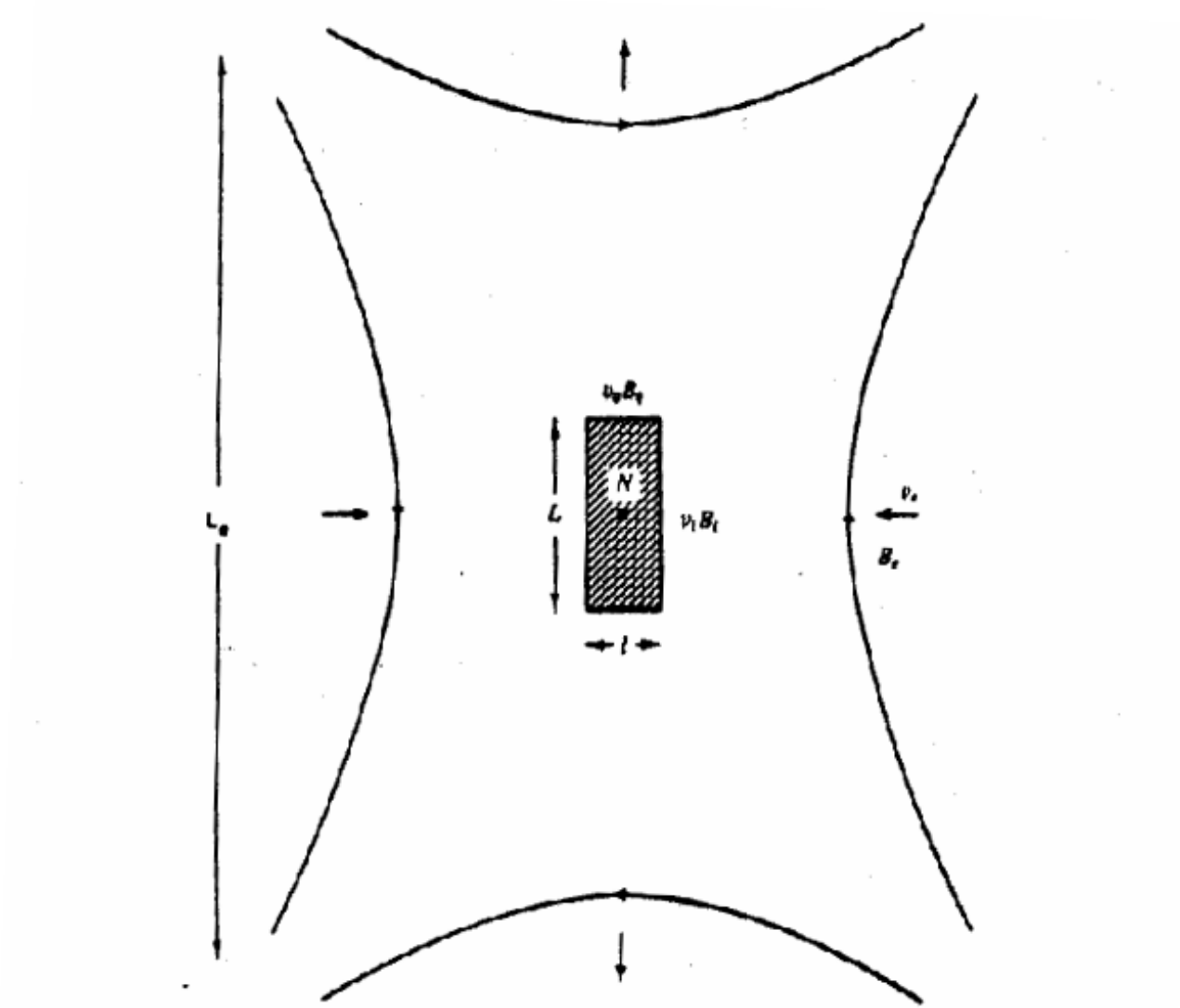

Fig. 10.3. The configuration for steady magnetic reconnection. Oppositely-directed field lines of strength B_0, frozen to the plasma, are carried towards one another at a speed v_0 by a converging flow. They enter a diffusion region (shaded) with dimensions l and L, are reconnected at the neutral point (N), and are finally ejected from the ends.

$$v_i = \frac{\eta}{l}, \tag{10.9}$$

$$\rho_i v_i L = \rho_e v_0 l. \tag{10.10}$$

Equation (10.8) arises because plasma is accelerated away from N by an excess gas pressure of amount $B_i^2/(2\mu)$, so that the outflow speed is a hybrid Alfvén speed, based on the inflow field and the current sheet density; Equation (10.9) expresses a balance between inwards convection and outwards diffusion; Equation (10.10) is a consequence of mass conservation. It can be seen from Equations (10.8) and (10.10) that $l \ll L$ provided $v_i \ll v_A^*(\rho_e/\rho_i)$.

In most applications the incompressible limit ($\rho_e = \rho_i$) has been adopted, on grounds of simplicity, so that Equations (10.8) to (10.10) simply determine v_0 and the dimensions of the diffusion region in terms of prescribed input values (v_i and B_i). However, when there is an appreciable temperature difference between the diffusion region and its surroundings, the density ratio (ρ_e/ρ_i) differs from unity. For a thin diffusion region ($l \ll L$), it is determined from the constancy of total pressure across the region, namely

$p_c = p_i + B_i^2/(2\mu)$, as

$$\frac{\rho_c}{\rho_i} = \frac{T_i}{T_c}(1 + \beta_i), \tag{10.11}$$

in terms of the inflow beta $\beta_i = p_i 2\mu/B_i^2$. Thus, for given inflow parameters, Equations (10.8) to (10.11) determine the outflow values (v_0, l, L, ρ_c) in terms of the current

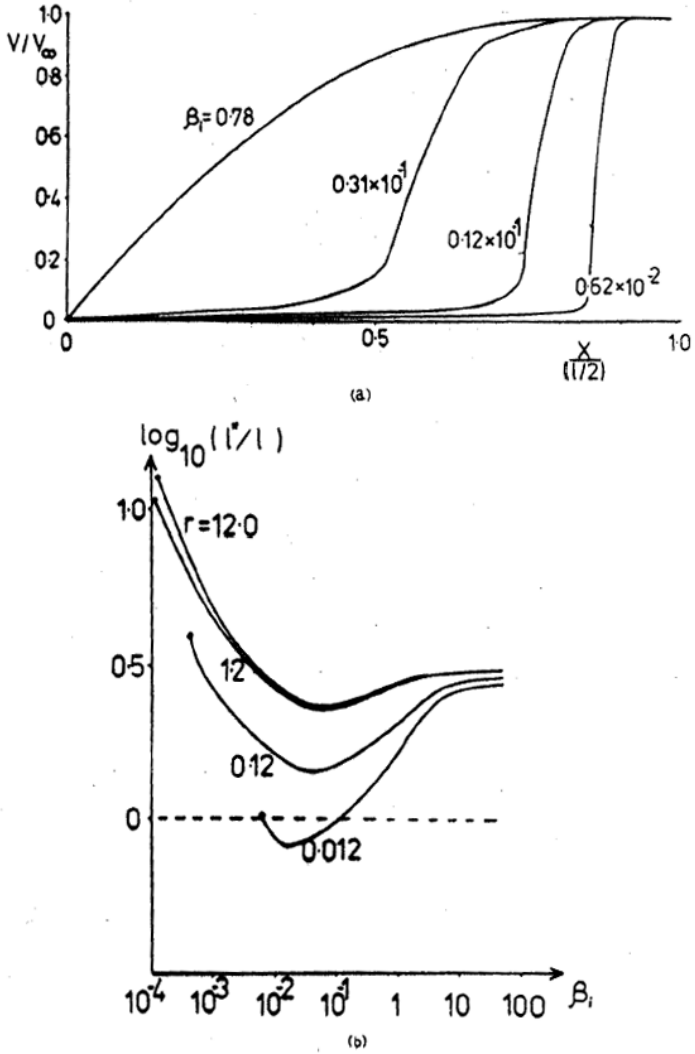

Fig. 10.4. The model of Milne and Priest (1981) for the central diffusion region. (a) The inflow speed as a function of distance (x) from the sheet centre for various values of β_i and $r = 0.012$ (β_i is the ratio of plasma to magnetic pressure for the inflow and r is the ratio of radiation to convection.) (b) The width (l^*) of the region in terms of its order-of-magnitude value ($l = \eta/v_i$).

Simple Loop Flares

- It is most likely due to new flux emergence (Fig10.7).
- There are 3 phases

(1) Preflare phase: emerging flux reconnects with outlines fields, shock waves radiate from a current sheet and heat the plasma.

(2) Impulsive phase: on set of turbulence in current sheet caused rapid expansion: E field accelerates particles

- Downward ---- Halpha, Hard X-ray
- Upward ---- radio Type IV bursts

(3) Main phase: both heat and particles are conducted down to lower chromosphere.

- Condition for onset of flare:

$$T_c^2 > T_{turb}^2 = 1.8 \times 10^{16} B_i/V_i$$

When current sheet reaches a critical height current density reaches a certain value to trigger to flare

Priest et. al. shows variation of critical height as a function of B_i and V_i

- Next, treat flare by two models:

Thermal Nonequilibrium and Instabilities

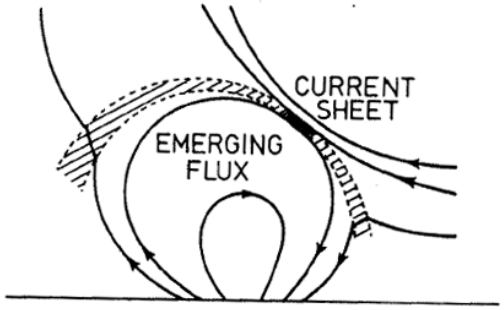

(a) Preflare Heating

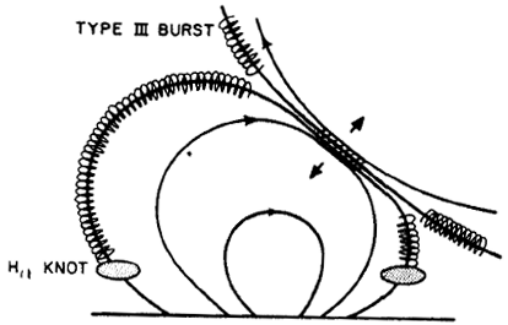

(b) Impulsive Phase

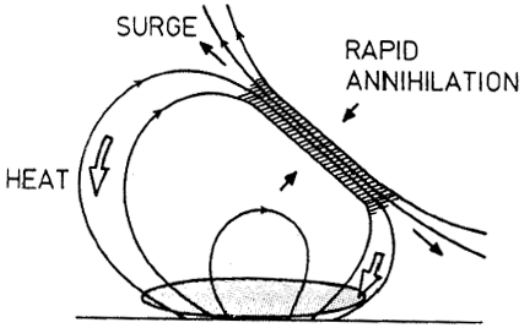

(c) Main Phase

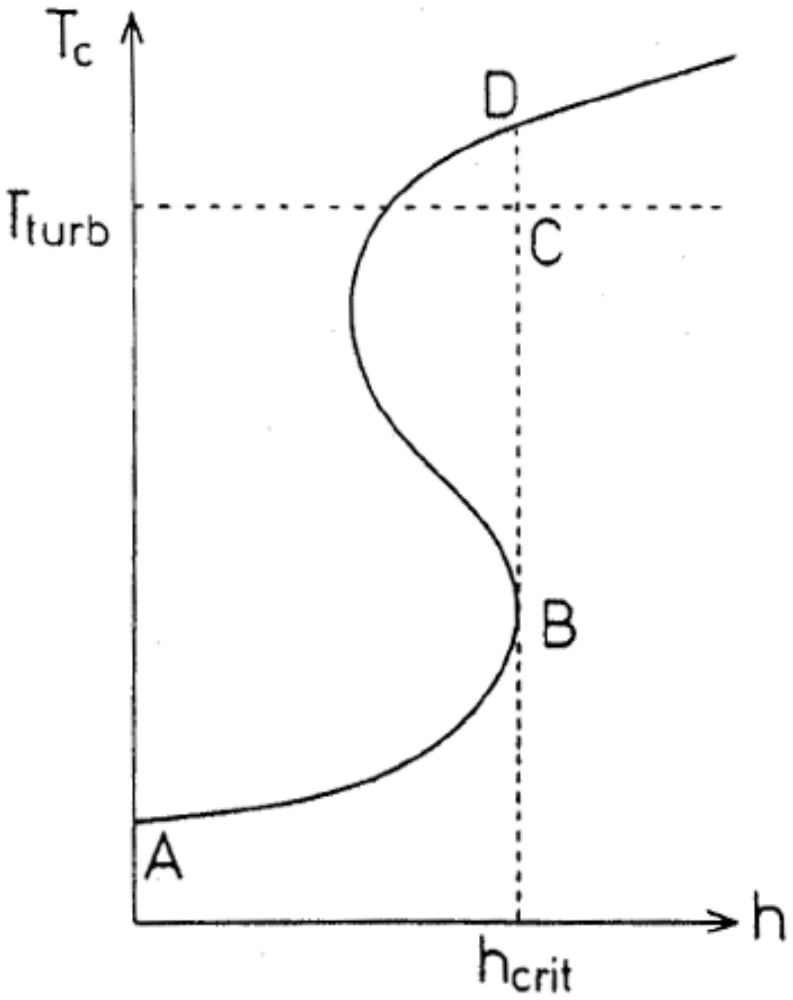

Fig. 10.8. The thermal equilibrium temperature (T_e) in a reconnecting current sheet is shown schematically as a function of height (h) in the solar atmosphere. As the sheet gains in height, the equilibrium solution moves along AB. When the critical height (h_{crit}) is attained, there are no neighbouring equilibria, and the sheet heats up dynamically along the path BD. But, as the temperature T_{turb} is exceeded, the critical current density for turbulence onset is surpassed.

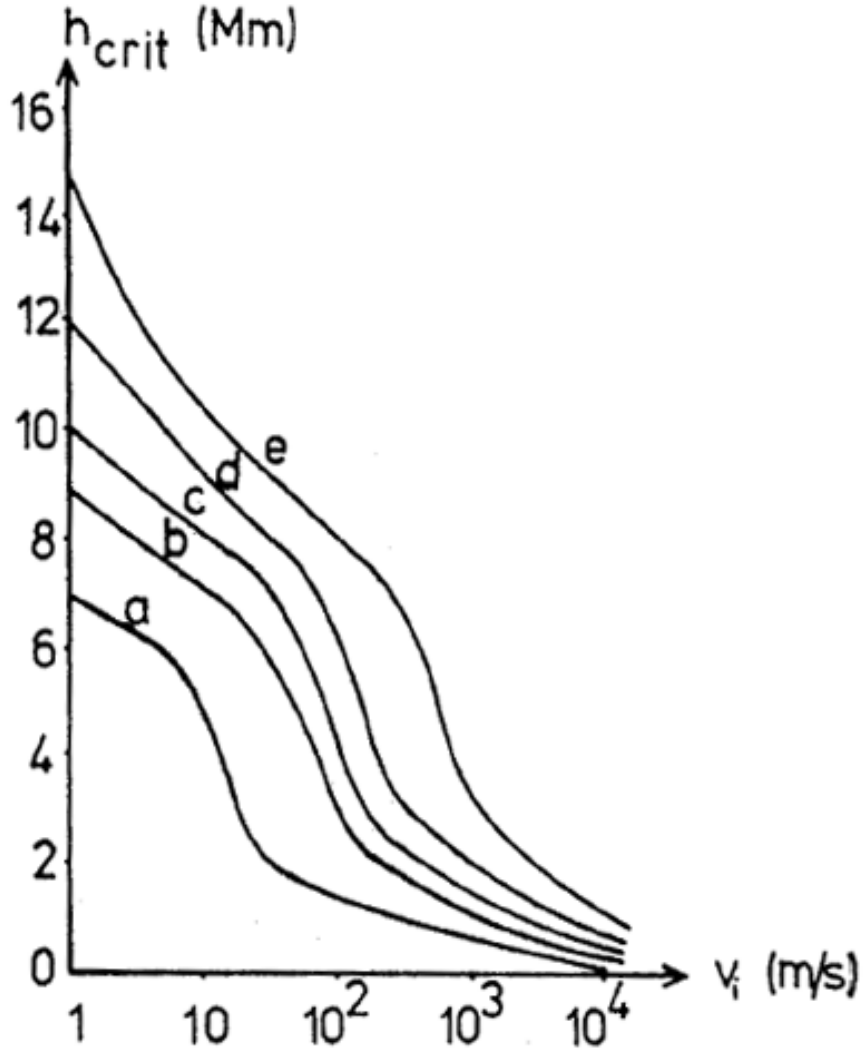

Fig. 10.9. The variation of the critical height (h_{crit}) in Mm (1 Mm = 10^6 m) for simple-loop flare onset with the emergence speed (v_i) for several values of the ambient magnetic field (B_i) in tesla. a, b, c, d, e refer to $B_i = 10^{-1}$, $10^{-1.5}$, 10^{-2}, $10^{-2.5}$, 10^{-3}, respectively. (A weakly turbulent diffusivity that is a 100 times larger than the classical value has been adopted) (from Milne and Priest, 1981).

Thermal Nonequilibrium

- Normally, magnetic fields are considered as the source of flare energy, but thermal non-equilibrium could occur in the core of an active region to cause flux.

$$10^4\ \mathrm{K} \xrightarrow{\text{heating}} 10^7\ \mathrm{K}$$

plasma

It may be a simple loop flare or a trigger for two-ribbon events (pre-flare heating)

- This phase is metal stable
- A simple static equation of equilibrium:

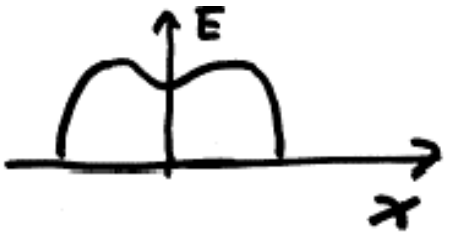

$$\frac{d}{ds}\left(k_0 T^{5/2}\frac{dT}{ds}\right) = n_e^2 Q(T) - H$$

Conduction optically thin radiation Heating

Fig 10-10 shows that when H reaches a critical value heating occurs along the dashed line.

Kink Instability

- Magnetic fields are unstable when twisted. The dominant stability effect is line-tying of ends of loop in dense photosphere. So we introduce the value critical twist Φ_c

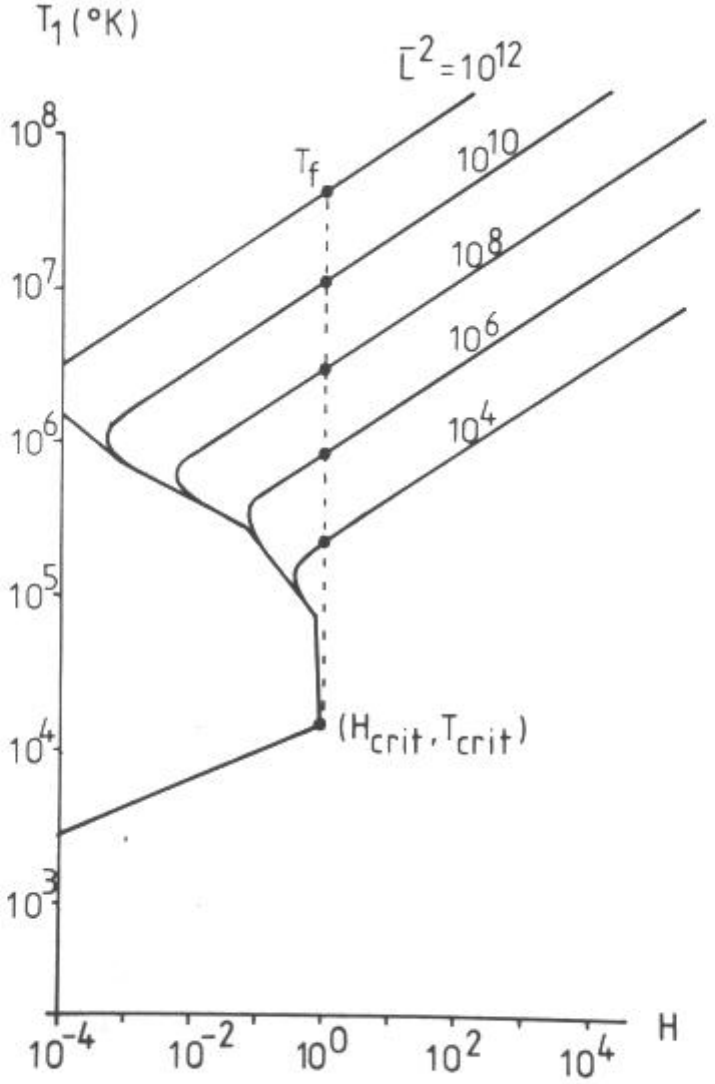

Fig. 10.10. The equilibrium summit temperature (T_1) of a loop as a function of the heating H (expressed in units of the radiative loss at $T = 2 \times 10^4$ K and $n_e = 5 \times 10^{14}\ m^{-3}$), for various values of the dimensionless half-length ($\bar{L} \equiv (Q/(\kappa_0 T^{7/2}))^{1/2} n_e L$) (from Hood and Priest, 1981a).

where $n_e = p/(2k_B T)$, and the pressure is uniform. Here s is the distance measured along a field line, $\mathrm{d}/\mathrm{d}s(\kappa_0 T^{5/2}\,\mathrm{d}T/\mathrm{d}s)$ represents conduction along the field (see (2.33)), and $n_e^2 Q(T)$ is the optically thin radiation (2.35c). Also, H is the heating term, which is assumed to be uniform per unit volume, although the qualitative features of the solution are not strongly dependent on its form (Section 6.5.1). The summit temperature (T_1) of the loop depends on the pressure (p), the heating (H) and the loop length ($2L$). The way in which T_1 depends on H and L for a fixed p is shown in Figure 10.10 when the conduction term is replaced by an order-of-magnitude approximation. As the heating rate slowly increases, so the summit temperature increases through equilibria on the lower branch. But, when the heating exceeds a critical value (H_{crit}), there is no longer a neighbouring equilibrium, and so the plasma rapidly heats up along the dashed line towards a quasi-steady flaring value (T_f) above 10^6K, denoted by a dot.

Similar results are obtained in several other cases: with different forms of heating; with full (rather than order-of-magnitude) solutions to (10.21); and with the effect of gravity incorporated. A lack of equilibrium can also be produced if the pressure is reduced. Finally, it must be pointed out that T_f is only a rough estimate of the flaring temperature; its value and the transition from the low- to the high-temperature state depend on the detailed plasma dynamics (Craig, 1981), which need to be studied in more detail.

- Consider a cylindrical flux tube with length 2L.

  Force balance: $$0 = \frac{dp}{dr} + \frac{d}{dr}\left(\frac{B_\phi^2 + B_z^2}{2\mu}\right) + \frac{B_\phi^2}{\mu r}$$

  Suppose solution $$\xi = [\xi^R(R), -i\frac{B_z}{B}\xi^0(R), i\frac{B_\phi}{B}\xi^0(R)]\cos\frac{\pi z}{2L}e^{i(m\phi+kz)}$$

  $$The \quad \delta W = \frac{1}{\mu}\int_0^\infty F\left(\frac{d\xi^R}{dR}\right)^2 - G\xi_R^2 dR$$

  F.G are function of R, p, B_ϕ , B_z, k defined in p262

  Solving *Euler-Lagrange equation*, subject to

  $$\xi^R = 1 \quad \frac{d\xi^R}{dR} = 0 \quad at \quad R = 0, for \quad m = 1$$

  $$\xi^R = 0 \quad \frac{d\xi^R}{dR} = 1 \quad at \quad R = 0, for \quad m \neq 1$$

- Fig 7.8 gave a sample solution
- Another example uniform axial field, $B_z=B_0$

$$\text{twist}: \quad \Phi(R) = \frac{2LB_\phi}{RB_z} = \frac{\Phi_0}{1+R^2/a^2}$$

$$p(R) = p_\infty + \left(\frac{\Phi a}{2L}\right)^2 \frac{B_0^2}{2\mu}$$

- Fig 10.11 gives a summary of instability.

  In the absence of pressure gradient and line-tying the critical twist:

$$\frac{1}{2}\Phi(0) = -\frac{2L}{a}\bar{k}$$

This is called *Kruskal-Shafranov limit*

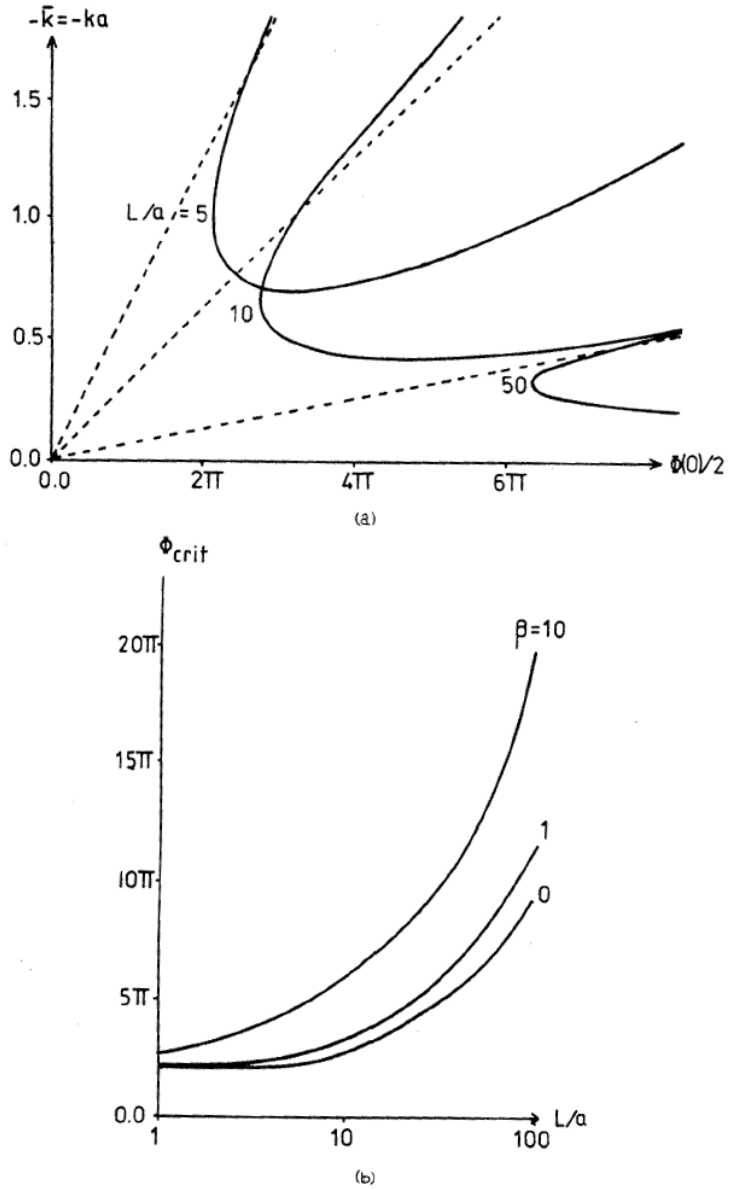

Fig. 10.11. Kink instability ($m = 1$) of a variable-twist field, with $\beta \equiv 2\mu p_\infty / B_0^2$, where p_∞ is the coronal pressure and B_0 is the uniform axial field. (a) The stability diagram for $\beta = 0$ and for different values of the aspect ratio (L/a). The equilibrium is stable to the perturbation (10.23) to the left of each curve and unstable to the right. $\frac{1}{2}\Phi(0)$ is the twist at $R = a$, the 'edge' of the loop. (b) The variation of the critical twist (Φ_{crit}) at $R = a$ with L/a and β (from Hood and Priest, 1979b).

Resistive Kink Instability

In most of cases, resistive term in the linearised induction equation:

$$\frac{\partial B_1}{\partial t} = \nabla \times (\vec{v}_1 \times \vec{B}_0) - \nabla \times (\eta \nabla \times B_1)$$

is negligible because R_m is large but in a layer

$$\nabla \times (\vec{v}_1 \times \vec{B}_0) = 0$$

$\frac{\partial \vec{B}}{\partial t}$ can no longer be balanced by $\nabla \times (\vec{v}_1 \times \vec{B}_0)$

For incompressible medium, $\nabla \cdot \vec{v}_1 = 0$ the locations of the singular layers are given by $\vec{k} \cdot \vec{B}_0 = 0$ if $v_1 = e^{i\vec{k}\cdot\vec{r}}$.

The simplest force free equilibrium in cylindrical geometry is constant α field:

$$B_\phi = B_0 J_1(\alpha R) \qquad B_z = B_0 J_0(\alpha R)$$

Its stability may be investigated by seeking solution

$$B_1 = B_1(R) \exp(\omega t + i(m\phi + kz))$$

Assuming that there is no line-tying --- *resistive internal kink mode*, the fasted growing perturbations have long wavelength $k \cdot R_s << 1$ and $m = 1$ grow rate:

$$\omega \approx \left[R_s^2 \left| (\vec{k} \cdot \vec{B})'_s \right| / B_0 \right]^{2/3} \tau_d^{-1/3} \tau_A^{-2/3}$$

$\tau_d = R_s^2 / n$ diffusion time

$\tau_A = R_s / v_A$ Alfven travel time

Two-Ribbon Flares

- A magnetic arcade responds to the slow photospheric motion of its foot point by evolving through a series of force-free equilibria. A some critical amount of shear, the configuration becomes unstable and erupts upwards (Fig 10.10).

- We also have two approaches:

  multiplicity of force-free equilibria and instability.

Existence and Multiplicity of Force-Free Equilibria

- Evolution through a set of equilibria, it may erupt if a neighbouring equilibrium ceases to exist or a new equilibrium with low energy becomes possible.
- Coronal arcade can be treated as 2-D force-free fields, independent of longitudinal coordinate. Say with components:

$$B_x(x,y)=\frac{\partial A}{\partial Z} \qquad B_z(x,y)=-\frac{\partial A}{\partial x} \qquad B_y(A)$$

$$\text{eq. 3.55} \qquad \nabla^2 A+\frac{d}{dA}\left(\frac{1}{2}B_y^2\right)=0$$

Using boundary condition, we can solve this equation and obtain the evolution of fields.

- Fig10.15 gave a sample solution

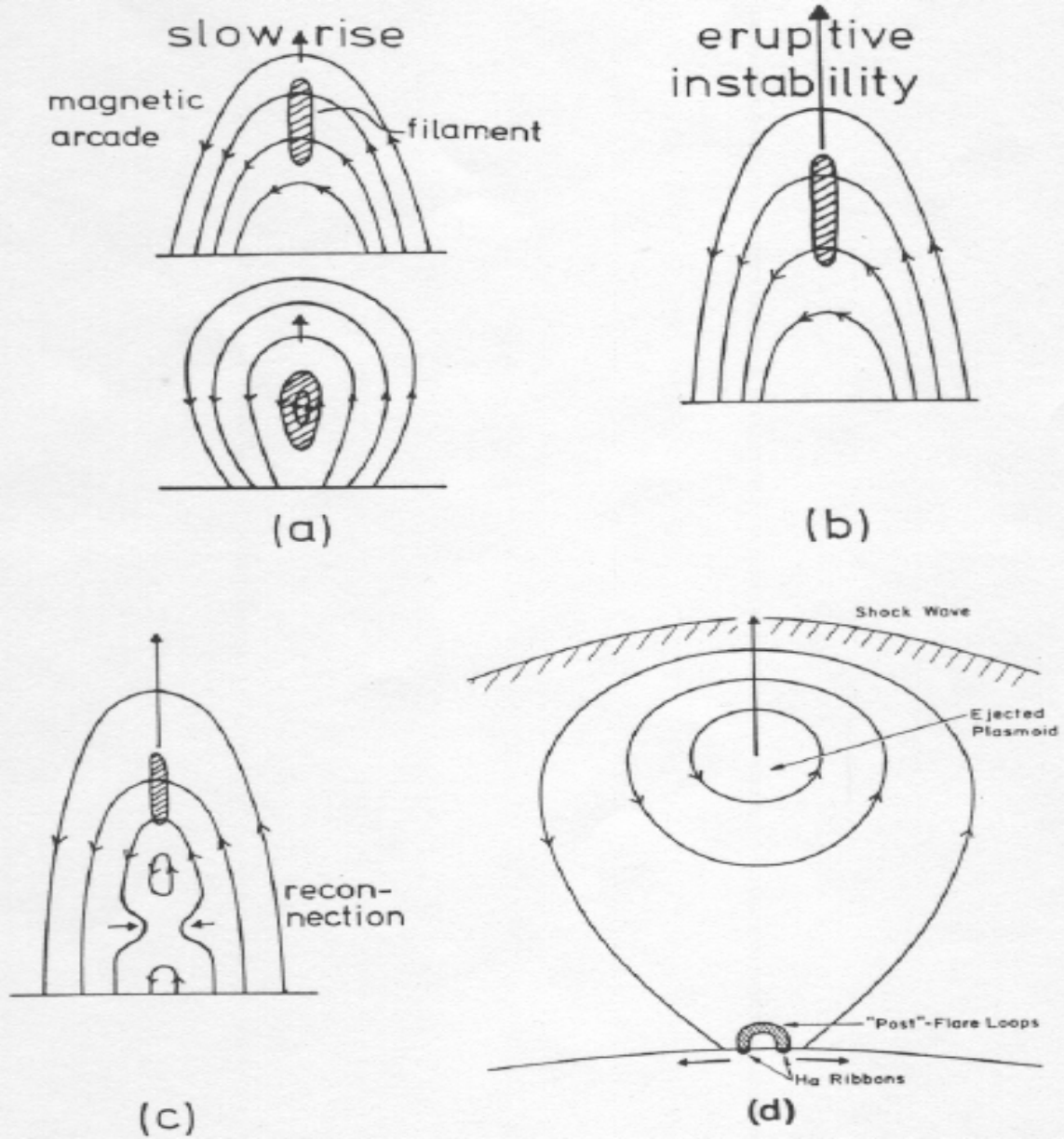

Fig. 10.12. The overall magnetic behaviour in a two-ribbon flare, as seen in a section through the magnetic arcade. (a) Slow preflare rise of a filament, possibly due to thermal nonequilibrium, emerging flux or the initial stages of an MHD instability. The surrounding field may just be sheared (upper diagram) or it may contain a magnetic island so that the filament lies along a flux tube (lower diagram). (b) Eruptive instability of a magnetic arcade and filament. (c) Field lines below the filament are stretched out until reconnection can start. (d) As reconnection proceeds, 'post'-flare loops rise and Hα ribbons move apart.

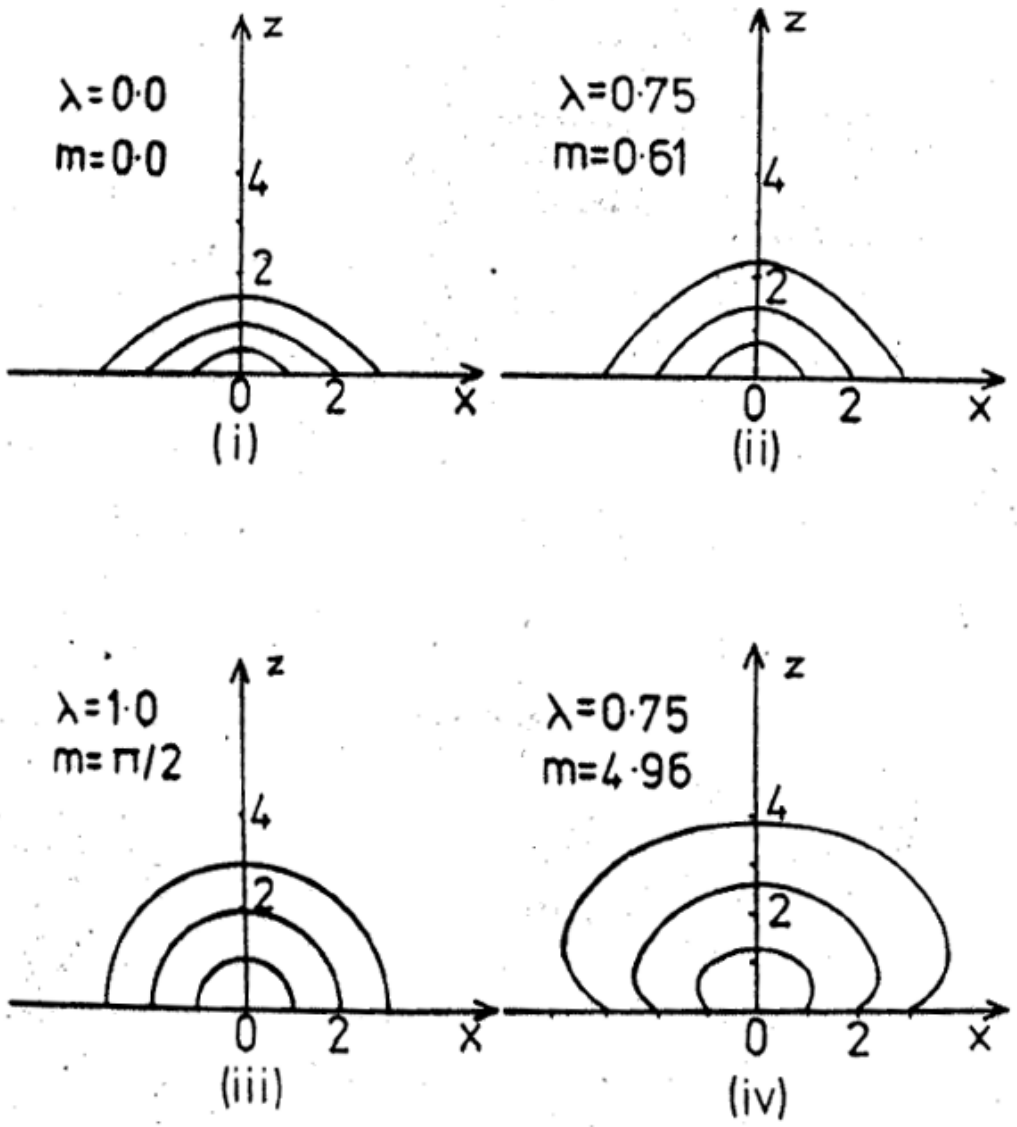

Fig. 10.15(a). The projections onto the vertical (x, z) plane of the field lines for the force-free solutions (10.32) of Priest and Milne (1980) with $k = -\frac{1}{2}$. As the shear gradient (m) increases, so λ increases to a maximum of 1 and then it decreases.

a distance h above and below the photosphere (Figure 10.16). For both of these fields the normal component at the photosphere is the same, namely

$$B_n(x) = \frac{x}{R_0} B_\phi(R_0), \tag{10.33}$$

where $R_0 = (h^2 + x^2)^{1/2}$. The photospheric shears, however, are different; they are defined here as the Z-separation of the two footpoints of a field line, and may be written

$$d^{(1)}(x) = 2\tilde{\Phi} R_0 \frac{B_z^{(1)}(R_0)}{B_\phi(R_0)} \tag{10.34}$$

and

$$d^{(2)}(x) = 2(\pi - \tilde{\Phi}) R_0 \frac{B_z^{(1)}(R_0)}{B_\phi(R_0)}, \tag{10.35}$$

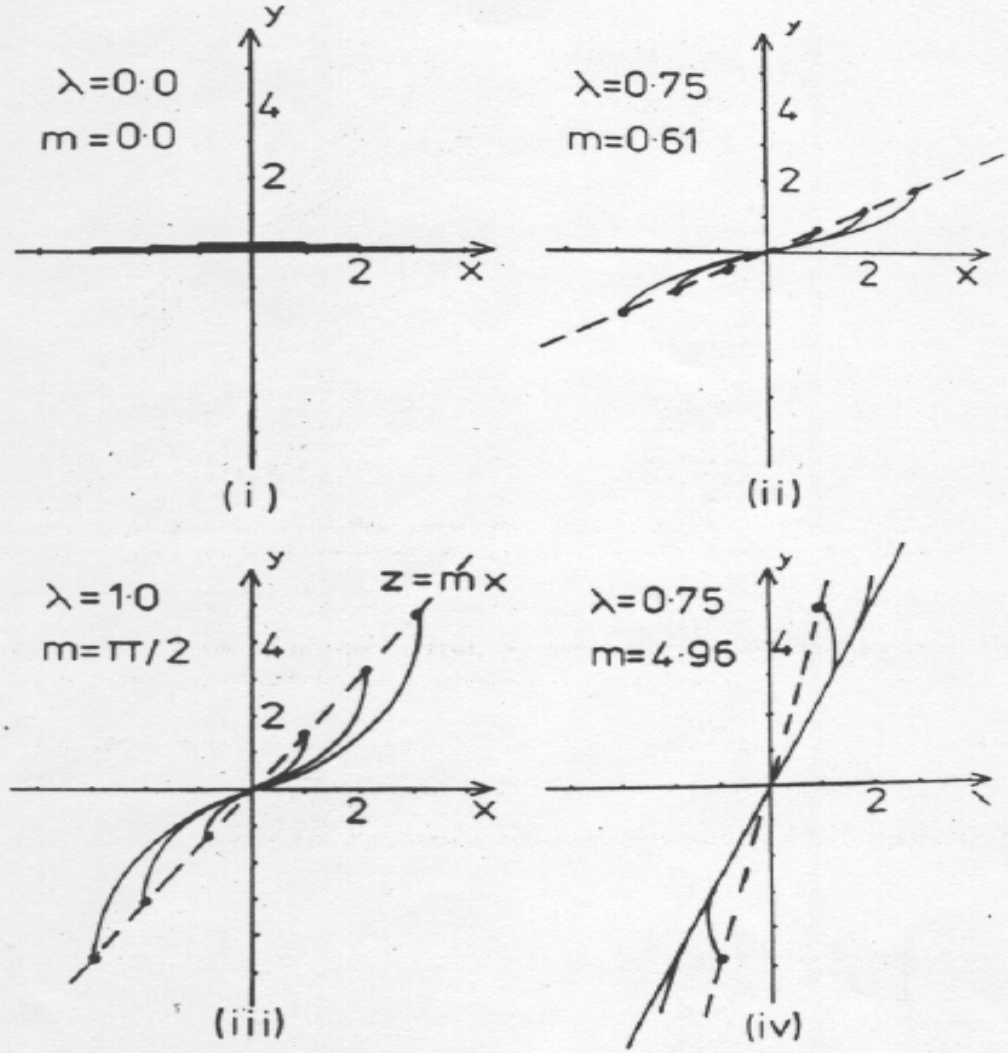

Fig. 10.15(b). The corresponding field-line projections onto the horizontal (x, y) plane. The dashed line $y = mx$ gives the location of footpoints initially lying on the x-axis.

where the inclination $\bar{\Phi}(R_0)$ of the radius vector to a field-line footpoint is given by $\cos \bar{\Phi}(R_0) = h/R_0$. Since the fields are force-free, both $B_z^{(1)}$ and $B_z^{(2)}$ satisfy

$$\frac{\mathrm{d}}{\mathrm{d}R}\left[\frac{B_\phi^2 + B_z^2}{2}\right] + \frac{B_\phi^2}{R} = 0. \tag{10.36}$$

Whole families of solutions to Problem I may now easily be constructed by just

Eruptive Instability

Fig 10.17(a) shows preflare condition--- a weakly twisted flux tube anchored at its end. A flare loop is at distance d above photosphere, its length is 2L. The field can be represented by uniform twisted force-free field:

$$B_\theta = B_0(R/a)/(1+R^2/a^2) \quad B_z = \frac{B_0}{1+R^2/a^2} \qquad R << d$$

Sufficient conditions for instability are obtained by integrating an *Euler-Lanrange Equation*

d ↑ easier to be unstable Fig10.17(b)

Φ ↑ easier to be unstable

E.g. d=3b $\Phi \geq 4.2\pi$, unstable

$\Phi \leq 2\pi$, flux tube is table to all kink perturbations.

Post-flare loops

Kopp-Pneuman Model

↓ flare ribbons

Eruption Field line open reconnection one at a time

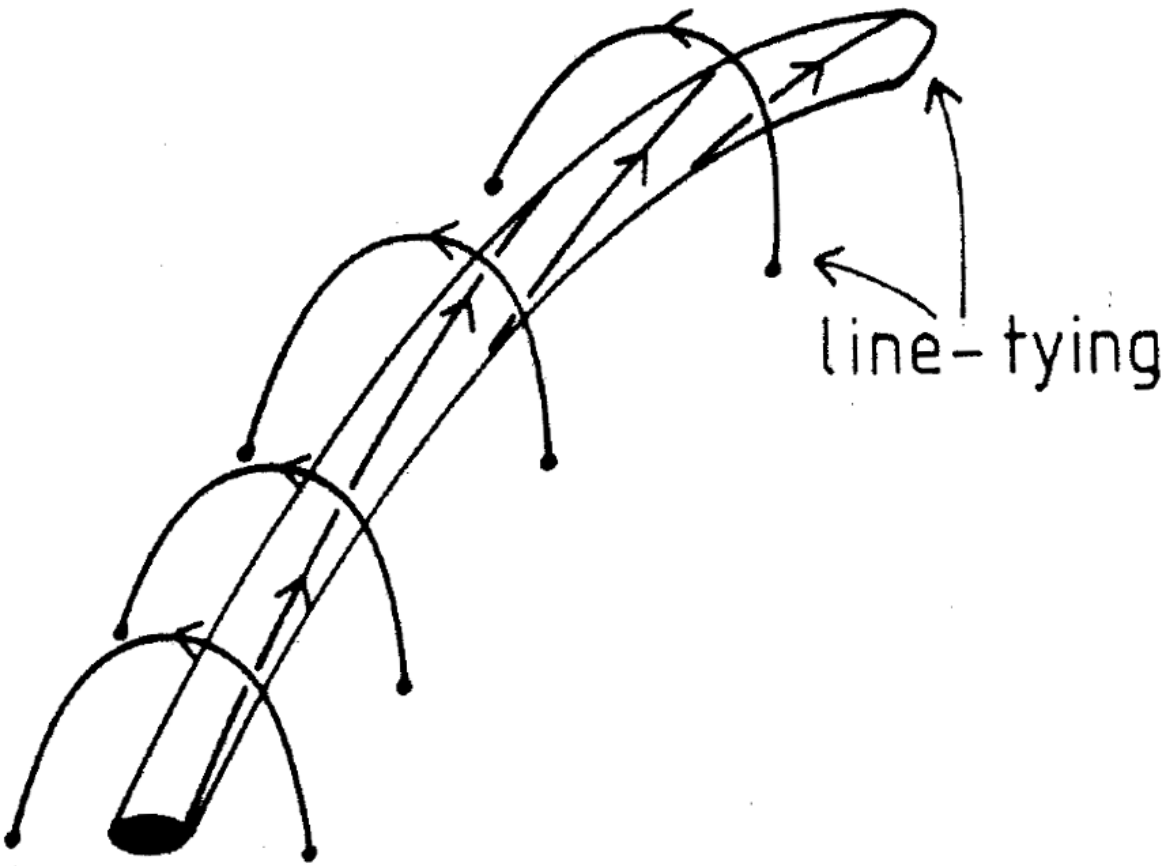

Fig. 10.17(a). A possible preflare configuration consisting of a weakly twisted flux tube anchored at its ends and located within a magnetic arcade. The plage filament is assumed to be located along the flux tube.

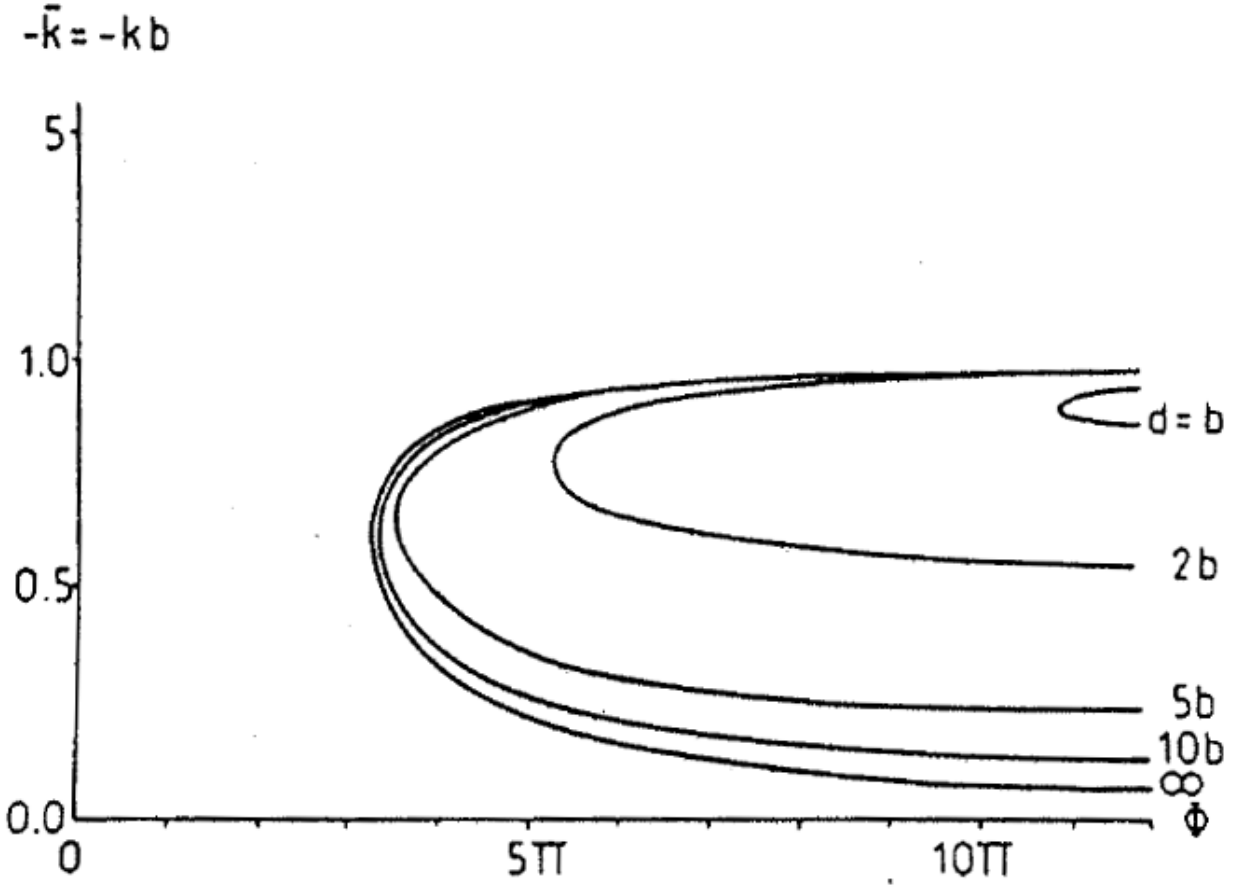

Fig. 10.17(b). Sufficient conditions for the amount of twist ($\Phi \equiv 2L/b$) required to produce instability of a flux tube embedded in an arcade. The flux tube has length $2L$, and its axis is situated at a height d above the photosphere. For Φ greater than some critical value (i.e., to the right of each curve), the equilibrium is unstable for a range of wavenumbers (k) (from Hood and Priest, 1980b).

1.4.4C). Examples can be seen in Figures 1.38 and 10.18. Cool Hα loops (with strong down-flows) are located below hot X-ray loops, which may reach an altitude of 100 000 km. The loop feet are rooted in two ribbons of Hα emission, which separate as the loops rise. The summit temperature and density early in the event may be as much as 10^7 K – 10^8 K and 10^{16} m^{-3}. Essentially the same phenomenon (but less energetic) occurs when a quiescent filament erupts without producing an Hα flare.

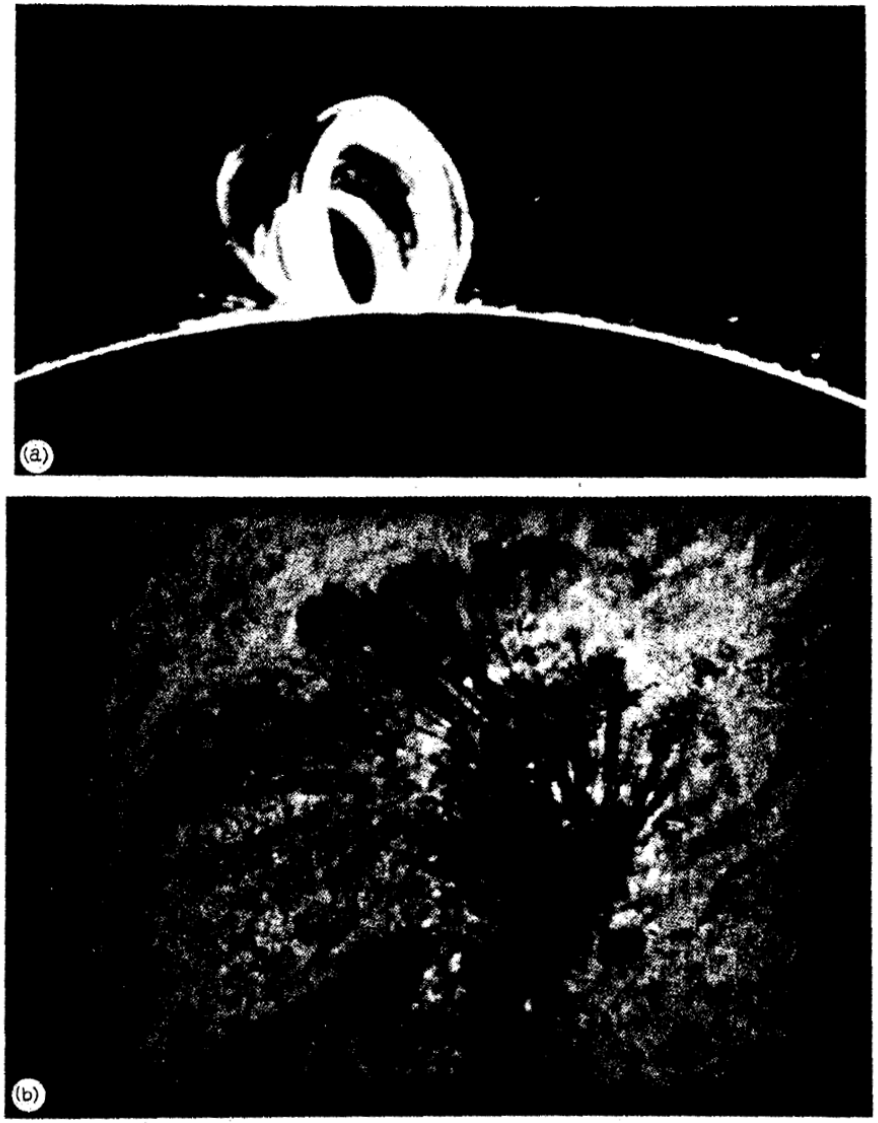

Fig. 10.18. Examples of cool 'post'-flare loops: (a) limb photograph in Hα; (b) disc photograph at Hα + 0.8 Å on 10 September, 1974 (© AURA Inc., Sacramento Peak Observatory).

Governing Equations:

$$\frac{Dv_s}{Dt}+v_s\frac{Dv_s}{Ds}=-\frac{1}{\rho}\frac{Dp}{Ds}-\frac{GM_\Theta}{r^2}\cos\alpha+v_n\frac{D\alpha}{Dt}+\frac{v_n^2}{r}\cos\alpha+\frac{v_n v_s}{R_c}$$

$$\frac{D}{Dt}(\rho A)+\frac{D}{Ds}(\rho v_s A)-\frac{\rho v_n A}{R_c}=0$$

R_c: radius of curvature of field line.

A: cross section. α: inclination to magnetic fields

Solution:

$$B_r=B_0\frac{1+2(r_1/r)^3}{1+2(r_1/R_\Theta)^3}\sin\theta \qquad B_\theta=-B_0\frac{1-(r_1/r)^3}{1+2(r_1/R_\Theta)^3}\cos\theta$$

neutral point location

$$r_1(t) = (1.5 - 0.5e^{-\omega t})R_\Theta$$

$$\omega = 5.7 \times 10^{-5} s^{-1} \text{ at } \quad r_1 = R_\Theta \quad \frac{dr_1}{dt} = 20 km/s$$

$$t = \infty \qquad r_1 = 1.5R_\Theta$$

when a tube closed (reconnects), a shock propagates downward, plasma cools and falls to give Hα loops.

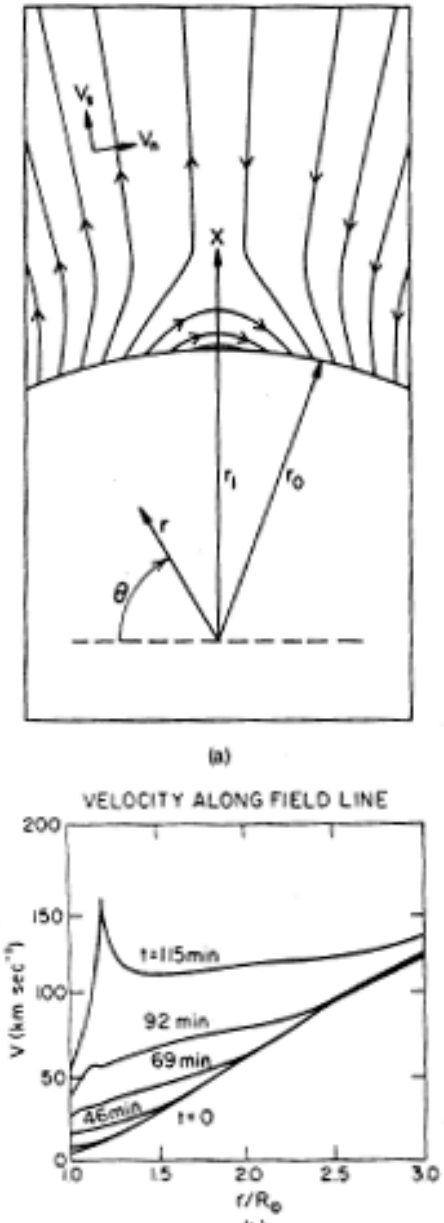

Fig. 10.19. The Kopp–Pneuman model of 'post'-flare loops: (a) field configuration and notation; (b) velocity versus radial distance along a moving flux tube that is swinging over from a vertical location towards the neutral point, which it reaches at $t = 115$ min at a height of 0.2 $R_\odot$ above the solar surface (from Pneuman, 1980).

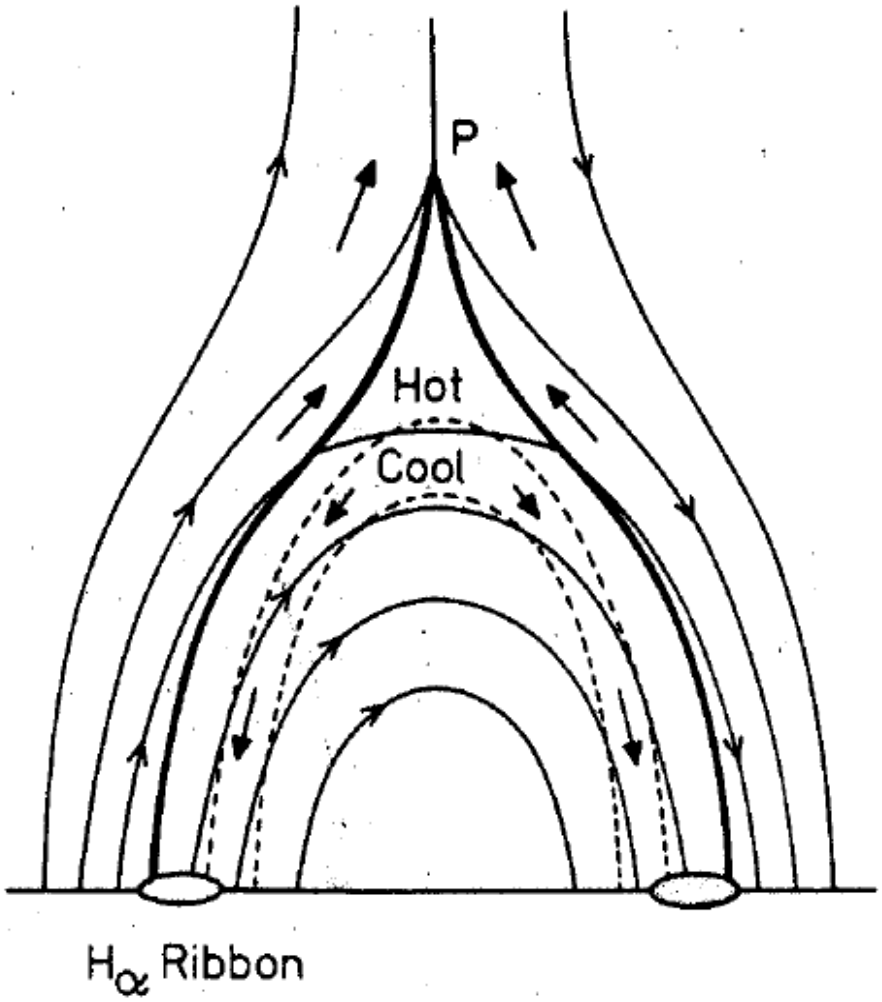

Fig. 10.20. The magnetic structure during the main phase of a two-ribbon flare. Plasma motions are indicated by dark-headed arrows, and the thick curve shows the position of the slow shock wave which trails from the rising neutral point *P* and brings the plasma to rest to form hot loops. When the plasma cools it falls and produces the cool loops outlined by dashed curves.

The shock is modelled for simplicity by Kopp and Pneuman as a *hydrodynamic shock*, but the resulting temperature rise (by a factor of 1.8) is not sufficient to explain the observed temperatures, especially early in the event. But Cargill and Priest (1982a) have shown that the extra release of energy from the magnetic field in a *slow magneto-acoustic shock* can provide the necessary heating. They find that the flare temperature depends on the value of the ambient plasma beta (β); for $\beta = 0.1$ the plasma is heated by the shock to typically 10^7 K, but for $\beta = 0.01$ the temperature can become even larger, as observed on the Solar Maximum Mission Satellite.

The mass flow is enhanced over the solar wind value by a factor of ten due to the field line motion. But the mass contained in a loop prominence system may be even larger than this flow would provide, and so the excess is probably supplied by chromospheric evaporation.

Since the above analysis is purely kinematic, it will be interesting in future to see the results of a completely magnetohydrodynamic simulation, including noniso-thermality, shock waves and evaporation.

Homework

Assume that reconnection between two magnetic dipoles causes a flare. Construct a reasonable model to (1) Estimate energy release due to the reconnection; (2) Plot electric current distribution before and after the flare.